PRAMANA
— journal of
physics

Vol. 62, No. 2
February 2004
pp. 347–358

Experimental and phenomenological status of neutrino anomalies

SANDIP PAKVASA
Department of Physics and Astronomy, University of Hawaii, Honolulu, HI 96822, USA
Email: pakvasa@phys.hawaii.edu

Abstract. The current status of neutrino anomalies is summarized; the KamLAND experiment is described and the recent results of KamLAND presented.

Keywords. Solar neutrino; reactor neutrino.

PACS Nos 96.40.Tv; 14.60.Pq

1. Introduction

The title of this talk is as assigned to me by the conference, and I will stick to it loosely. I will be somewhat selective and cover only a few topics. My plan is as follows: (i) review the atmospheric neutrinos, including a brief history as well as the (ii) recent K2K results; (iii) be very brief, in solar neutrinos in view of Goswami's talk [1]; (iv) present KamLAND results; (v) review LSND and (vi) conclude.

Now that neutrino oscillations are well-established as the primary explanation for both solar and atmospheric neutrino results, it seems to me that it is time to stop referring to them as 'anomalies'. I propose that the phrase 'neutrino anomaly' should henceforth be reserved for observations that *cannot* be accounted for in terms of neutrino oscillations; for example 'the NUTeV Anomaly' [2].

2. Atmospheric neutrinos

Cosmic ray primaries interact with nuclei at the top of the atmosphere and produce neutrinos via the $\pi \to \mu \to e$ chain. In the energy range (below about 10 GeV) where all the $\mu's$ decay, the ν_μ/ν_e ratio is nearly 2/1; and above that energy there are very few $\nu_e's$. The absolute fluxes are somewhat uncertain, but known to within 20%.

The earliest experiments to detect atmospheric neutrinos were the Kolar Gold Field (KGF) and the Case–Witwatersrand–Irvine (CWI) detectors built in the early sixties. The KGF detector in South India used a set of telescope counters consisting of iron, flash tubes and scintillation. The neutrino events could be separated from

downward going muons at zenith angles higher than 60°. Eventually 100 contained events and 229 ν induced horizontal $\mu's$ were recorded. In 1965, KGF was the first to report and publish the neutrino events [3]. However, the first recorded atmospheric neutrino event was detected by CWI on 23 February 1965 (beating KGF by about a month!), also relying on the zenith angle as a signature [4].

Even though the absolute neutrino fluxes and cross-sections had large uncertainties, already by early seventies there were hints that the recorded ν_μ events were too few, some factor of two off from expectations [5]. This was the first hint of an atmospheric neutrino anomaly. In 1980, several groups presciently included the factor of two anomaly in atmospheric $\nu'_\mu s$ in a list of possible neutrino anomalies demanding an explanation [6].

The modern re-incarnation of this anomaly begins with the observation by IMB in 1986 that the number of events with visible μ-e decay were too few [7]. They did not pursue this discrepancy with much vigor. In 1988, Kamiokande published their results on the deviation of μ/e event ratio from the expected value of 2/1 [8]. Several groups immediately interpreted these results in terms of neutrino oscillations ($\nu_\mu \to \nu_e$ or $\nu_\mu \to \nu_\tau$) and deduced the range of mass difference and mixing needed to account for the data [9]. In 1992, IMB published a paper in which it was claimed that by combining contained as well as partially contained events a large region in parameter space was excluded [10]. This included not only the parameter range favored by Kamiokande results but also the now established Super-K region! (The results of this paper have not yet been officially retracted.) Also in 1992, Kamiokande published results from an analysis covering a larger energy range showing some variation with L/E in accord with expectations from oscillations but with poor statistics [11].

There were also the lingering problems from the lack of evidence from detectors using different techniques. Then in 1996, Super-Kamiokande began taking data. As far back as 1979, a technique to use the up–down asymmetry of ν_μ/ν_e ratio was proposed as a means of probing oscillations [12]. In 1980, this was improved upon; namely the proposal was now to use the up-down asymmetry of ν_μ and ν_e separately [13]. This technique had two advantages: it is less prone to experimental systematics and can be used to probe oscillations of ν_μ and ν_e into any channels. In 1998, Super-K utilized precisely this method to truly establish oscillations as the primary cause for the atmospheric neutrino anomaly and removed all doubts about the nature of the anomaly [14]. Subsequent analysis by Super-K established the following facts: (1) the best fit values for the mass and mixings are given by $\delta m^2 = 2.5 \times 10^{-3}$ eV^2 and $\sin^2 2\theta = 1$; (ii) there is no evidence of $\nu'_e s$ oscillating; and (iii) ν_μ seems to be oscillating primarily into ν_τ, at least 80% of the time [15]. Explanations based on other exotic phenomena are almost all ruled out. The only remaining caveat for the conventional mass-mixing explanation is that the dip in the survival probability (which is a hallmark of oscillations) has not yet been seen experimentally, simply due to lack of enough resolution in L/E. One would like to see such a dip eventually. On a final note, other non-water-Cherenkov detectors such as SOUDAN-II and MACRO do see the same phenomena and find good agreement with the Super-K favored parameter values [16].

3. K2K

The first long baseline experiment has just published its first results [17]. K2K (KEK to Kamioka) experiment utilizes the 12 GeV PS at KEK to produce $\nu'_\mu s$ and shoots the beam towards Super-K. The distance is about 250 km and E_ν is peaked at 1.3 GeV. The near detector at KEK to monitor the beam consist of 1 kt water Cerenkov and a fine grained water tube with scintillation fibre 6 ton detector. This way the neutrino flux is accurately known. The final result of the analysis of events observed in Super-K is a fit of the survival probability to δm^2 and $\sin^2(2\theta)$. The results are consistent with the Super-K atmospheric neutrino with larger errors. The next round of long baseline experiments should reduce the errors on mass-mixing parameters, observe the oscillation dip and detect $\nu'_\tau s$ in the final state.

4. Solar neutrino summary

I refer to Goswami's talk for a full discussion of analysis of solar neutrino data [1]. My own brief take of the situation is as follows [18].

The solar neutrino data indicate that solar ν_e oscillates into another neutrino. The parameters in the range of LMA, LOW and VAC are all still viable. Unconventional explanations, such as (i) FCNC-NUNC with no neutrino masses, (ii) Lorentz invariance violation and (iii) resonant-spin-flavor-precession with transition magnetic moment in the range of $10^{-11}\mu_{\rm B}$; are all still possible. (The situation after KamLAND is quite different, see below.) The SNO data on neutral currents go a long way to vindicate the SSM flux calculations. The sterile component in the final state is constrained to be less than about 40%.

5. KamLAND

The following account is based closely on the first publication of KamLAND results in Physical Review Letters [19]. The primary goal of the Kamioka Liquid scintillator Anti-Neutrino Detector (KamLAND) experiment [20] is a search for the oscillation of $\bar{\nu}_e$'s emitted from distant power reactors. The long baseline, typically 180 km, enables KamLAND to address the oscillation solution of the 'solar neutrino problem' with $\bar{\nu}'_e s$ under laboratory conditions. The inverse β-decay reaction, $\bar{\nu}_e + p \rightarrow e^+ + n$ is used to detect $\bar{\nu}_e$'s in liquid scintillator (LS) [21]. Detecting both the e^+ and the 2.2 MeV γ-ray from neutron capture on a proton in delayed coincidence is a powerful tool for reducing background.

KamLAND occupies the site of the earlier Kamiokande [22], under 2,700 m.w.e. resulting in 0.34 Hz of cosmic-ray muons in the detector. The neutrino detector/target is 1 kton of ultrapure LS contained in a 13 m diameter spherical balloon made of 135 μm thick transparent nylon/EVOH (ethylene vinyl alcohol copolymer) composite film. A network of Kevlar ropes supports and constrains the balloon. The LS is 80% dodecane, 20% pseudocumene (1,2,4-trimethylbenzene), and 1.52 g/l of PPO (2,5-diphenyloxazole) as a fluor.

A buffer of dodecane and isoparaffin oils between the balloon and an 18 m diameter spherical stainless-steel containment vessel shields the LS from external radiation. During filling water extraction and nitrogen stripping [23], purified the LS and buffer oil (B0). The buffer oil density is 0.04% lower than the LS. A 1879 photomultiplier tube array, mounted on the containment vessel, completes the inner detector (ID). There are 1,325 newly developed fast17 inch diameter photomultiplier tubes (PMTs) and 554 older Kamiokande 20 inch PMTs [24]. The total photo-cathode coverage is 34% but only the 17 inch PMTs 22% coverage are used for the present analysis. A 3 mm thick acrylic barrier at 16.6 m diameter reduces radon from PMT glass in the LS. The containment vessel is surrounded by a 3.2 kton water-Cherenkov detector with 225 20 inch PMTs. This outer detector (OD) absorbs γ rays and neutrons from surrounding rock and acts as a tag for cosmic-ray muons. The primary ID trigger threshold is 200 PMT hits, corresponding to about 0.7 MeV. The threshold goes to 120 hits for 1 ms after a primary trigger. The OD trigger threshold corresponds to $> 99\%$ tagging efficiency.

Energy response in the 0.5 to 7.5 MeV range is calibrated with ^{68}Ge, ^{65}Zn, ^{60}Co, and Am–Be gamma-ray sources deployed at various positions along the vertical axis. Detected energy is obtained from the number of observed photoelectrons (p.e.) after corrections for gain variation, solid angle, density of PMTs, shadowing by suspension ropes, and transparencies of the LS and BO. The observed energy resolution is $\sim 7.5\%/\sqrt{E(\mathrm{MeV})}$.

The energy scale is augmented from studies of the radiation from ^{40}K and ^{208}Tl and Bi–Po contaminants (as well as in the detector), Bi–Po sequential decays, the spallation products ^{12}B and ^{12}N, and γs from thermal neutron captures on protons and ^{12}C. The reconstructed energy varies by less than 0.5% within the 10 m diameter fiducial volume; local variations near the chimney region are about 1.6%. The energy scale exhibits less than 0.6% variation in time during the entire data run. Corrections for quenching and Cherenkov light production are included, and contribute to the systematic error. The estimated systematic error for the energy scale is 1.9% at the 2.6 MeV energy threshold which corresponds to a 2.1% uncertainty in the detected neutrino rate. Correlated decays from Bi–Po and ^{8}He/^{9}Li yield energies between 0.6 MeV and $\sim$15 MeV and are used to extend the range of the energy calibration.

The source positions are reconstructed from the relative times of PMT hits. Energy-dependent radial adjustments are used to reproduce the known source positions to $\sim$5 cm; the typical position reconstruction resolution is 25 cm. Vertex reconstruction performance throughout the LS volume is verified by reproducing the uniform distribution of 2.2 MeV capture γ's from spallation neutrons.

The data shown here were collected from March 4 through October 6, 2002. 370×10^6 events in 145.1 days of live time were collected at an average trigger rate of $\simeq$30 Hz. Events with fewer than 10,000 p.e. ($\sim$30 MeV) and no prompt OD tag are 'reactor-$\bar{\nu}_e$ candidates'; more energetic events are treated as 'muon candidates'.

The selection cuts for $\bar{\nu}_e$ events are the following: (i) fiducial volume cut ($R < 5$ m), (ii) time correlation cut ($0.5\ \mu\mathrm{s} < \Delta T < 660\ \mu\mathrm{s}$), (iii) vertex correlation ($\Delta R <$ 1.6 m), (iv) delayed energy ($1.8\ \mathrm{MeV} < E_{\mathrm{delay}} < 2.6\ \mathrm{MeV}$), and (v) a requirement that the delayed vertex position be more than 1.2 m from the central vertical axis

to eliminate background from thermometers. The overall efficiency for the events from criteria (ii)–(v) including the effect of (i) on the delayed vertex is (78.3±1.6)%.

Including annihilation, the detected energy for positrons is the kinetic energy plus twice the rest energy; thus e^+ from $\bar{\nu}_e$ events produce $E_{\rm prompt} = E_{\bar{\nu}_e} - \bar{E}_n - 0.8$ MeV, where $\bar{E}_n$ is the average neutron recoil energy. Anti-neutrinos emitted by ^{238}U and ^{232}Th decays in the Earth, 'geo-neutrinos' ($\bar{\nu}_{\rm geo}$), contribute low-energy events with $E_{\rm prompt} < 2.49$ MeV. For example, model Ia of $\bar{\nu}_{\rm geo}$ in [25] predicts about 9 $\bar{\nu}_{geo}$ events in our data set. However the abundances of U and Th and their distributions in the Earth are not well-known. To avoid ambiguities from $\bar{\nu}_{\rm geo}$'s we employ (vi) a prompt energy cut, $E_{\rm prompt} > 2.6$ MeV in the present analysis.

Low-energy γ-rays from ^{208}Tl ($\simeq$3 Hz) entering from outside the balloon are potential sources of background in the range up to 3 MeV and are strongly suppressed by the fiducial volume cut (i). The fiducial volume is estimated using the uniform distribution of spallation neutron capture events. The ratio of these events in the fiducial volume to those in the total volume agrees with the geometric fiducial fraction to within 4.06%. The same method is used for higher energy events, ^{12}N, ^{12}B β's following muon spallation, and agrees within 3.5%. Accounting for uncertainty in the LS total mass of 2.1%, we estimate the total systematic uncertainty of the fiducial volume to be 4.6%. The density of the LS is 0.780 g/cm^3 at 11.5°C; the hydrogen-to-carbon ratio is computed from the LS components to be 1.969 and was verified by elemental analysis (±2%). The specific gravity of the LS is measured to 0.01% precision using a commercial density meter, and we assign an additional 0.1% systematic error due to the uncertainty in the LS temperature. The 408 ton fiducial mass thus contains 3.46×10^{31} free target protons.

The trigger efficiency was determined to be 99.98% using LED light sources. The combined efficiency of the electronics, data acquisition, and event reconstruction was carefully studied using time distributions of uncorrelated events from calibration γ sources. We find that this combined efficiency is greater than 99.98%. The vertex fitter yields > 99.9% efficiency within 2 m of known source positions. Using calibrated ^{60}Co and ^{65}Zn sources, the overall efficiency was verified to within the 3% uncertainty in source strengths. The detection efficiency of delayed events from the Am–Be source (4.4 MeV prompt γ and 2.2 MeV delayed neutron capture γ within 1.6 m) was verified with 1% uncertainty.

From studies of Bi–Po sequential decays, the equilibrium concentrations of ^{238}U and ^{232}Th in the LS are estimated to be $(3.5 \pm 0.5) \times 10^{-18}$ g/g and $(5.2 \pm 0.8) \times 10^{-17}$ g/g, respectively. The observed background energy spectrum constrains the ^{40}K contamination to be less than 2.7×10^{-16} g/g. The accidental background, obtained from the observed flat distribution in the delayed time window 0.020–20 s, is 0.0086 ± 0.0005 events for the present data set.

At higher energies, the background is dominated by spallation products from energetic muons. We observe ~3,000 neutron events/day/kton. We also expect ~1,300 events/day/kton [26] for various unstable products.

Single neutrons are efficiently suppressed by a 2-ms veto following a muon, but care is required to avoid neutrons which mimic the $\bar{\nu}_e$ delayed coincidence signal. Most fast neutrons are produced by energetic muons which pass through both the OD and the surrounding rock. This background is evaluated by detecting delayed coincidence events with a prompt signal associated with a muon detected only

by the OD. As expected, a clear concentration of events near the balloon edge is observed. The expected background inside the fiducial volume is estimated by extrapolating the vertex position distribution and considering an OD reconstruction efficiency of 92%. To estimate the number of background events due to neutrons from the surrounding rock, the OD-associated rate is scaled by the relative neutron production and neutron shielding properties of the relevant materials. We estimate that the total fast neutron background is less than 0.5 events for the entire data set.

Most radioactive spallation products simply beta decay, and are effectively suppressed by requiring a delayed neutron signal. Delayed neutron emitters like ^{8}He ($T_{1/2} = 119$ ms) and ^{9}Li (178 ms) are eliminated by two time/geometry cuts: (a) a 2-s veto is applied for the entire fiducial volume following a showering muon (those with more than 10^6 p.e., $\sim$3 GeV, extra energy deposition), (b) for the remaining muons, delayed events within 2 s and 3 m from a muon track are rejected. The efficiency of these cuts is calculated from the observed correlation of spallation neutrons with muon tracks. The remaining ^{8}He and ^{9}Li background is estimated to be 0.94 ± 0.85. The dead time due to the spallation cuts is 11.4%. This method is checked by exploiting the time distribution of the events after a detected muon to separate the short-lived spallation-produced activities from $\bar{\nu}_e$ candidates. The uncorrelated $\bar{\nu}_e$ event distribution has a characteristic time constant of $1/R_\mu \simeq 3$ s, where R_μ is the incident muon rate. Spallation products have a much shorter time constant ($\sim$0.2 s). These methods agree to 3% accuracy. The total number of expected background events is 0.95 ± 0.99, where the fast neutron contribution is included in the error estimate.

Instantaneous thermal power generation, burn-up and fuel exchange records for all Japanese commercial power reactors are provided by the power companies. The time dependence of the thermal power generation data is checked by comparison with the independent records of electric power generation. The fission rate for each fissile element is calculated from these data, resulting in a systematic uncertainty in the $\bar{\nu}_e$ flux of less than 1%. Averaged over the present live-time period, the relative fission yields from the various fuel components are ^{235}U : ^{238}U : ^{239}Pu : ^{241}Pu = 0.568 : 0.078 : 0.297 : 0.057. The $\bar{\nu}_e$ spectrum per fission and its error (2.48%) are taken from the literature [27]. These neutrino spectra have been tested to a few per cent accuracy in previous short-baseline reactor $\bar{\nu}_e$ experiments [28]. The finite β-decay lifetimes of fission products introduce an additional uncertainty of 0.28% to the $\bar{\nu}_e$ flux; this is estimated from the difference of the total $\bar{\nu}_e$ yield associated with shifting the run time by one day. The contribution to the $\bar{\nu}_e$ flux from Korean reactors is estimated to be (2.46 ± 0.25)% from the reported electric power generation rates. Other reactors around the world give an average (0.70 ± 0.35)% contribution, which is estimated by using reactor specifications from the International Nuclear Safety Center [29]. The errors from reactors outside Japan are included in the table under 'reactor power'.

Although the anti-neutrino flux at the location of KamLAND is due to many nuclear reactors at a variety of distances, the $\bar{\nu}_e$ flux is actually dominated by a few reactors at an average distance of $\sim$180 km. More than 79% of the computed flux arises from 26 reactors within the distance range 138–214 km. One reactor at 88 km contributes an additional 6.7% to the flux and the other reactors are

more than 295 km away. This relatively narrow band of distances implies that for some oscillation parameters KamLAND can observe a distortion of the $\bar{\nu}_e$ energy spectrum.

The flux of anti-neutrinos from a reactor at a distance L from KamLAND is approximately proportional to the thermal power flux $P_{\rm th}/4\pi L^2$, where $P_{\rm th}$ is the reactor thermal power. The integrated total thermal power flux during the measurement live time is 254 J/cm^2. The systematic error assigned to the thermal power is conservatively taken as 2% from the regulatory specification for safe reactor operation. The corresponding expected number of reactor neutrino events (in the absence of neutrino oscillations) in the fiducial volume for this data set is 86.8 ± 5.6.

The space-time correlation of the prompt and delayed events is in good agreement with expectations, and the observed mean neutron capture time is 188 ± 23 μs. After applying the prompt and delayed energy cuts, 54 events remain as the final sample. The ratio of the number of observed reactor $\bar{\nu}_e$ events to that expected in the absence of neutrino oscillations is

$$\frac{N_{\rm obs} - N_{\rm BG}}{N_{\rm expected}} = 0.611 \pm 0.085({\rm stat}) \pm 0.041({\rm syst}).$$

The probability that the KamLAND result is consistent with the no disappearance hypothesis is less than 0.05%. The measured spectrum is consistent (93% confidence) with a distorted spectrum shape as expected from neutrino oscillations, but a renormalized no-oscillation shape is also consistent at 53% confidence.

The neutrino oscillation parameter region for two-neutrino mixing is shown in figure 1. The dark shaded area is the LMA region at 95% CL derived from [30]. The shaded region outside the solid line is excluded at 95% CL from the rate analysis with $\Delta\chi^2 \geq 3.84$ and

$$\chi^2 = \frac{(0.611 - R(\sin^2 2\theta, \Delta m^2))^2}{0.085^2 + 0.041^2}. \tag{1}$$

Here, $R(\sin^2 2\theta, \Delta m^2)$ is the expected ratio with the oscillation parameters.

The spectrum of the final event sample is then analysed with a maximum likelihood method to obtain the optimum set of oscillation parameters with the following χ^2 definition:

$$\begin{aligned}\chi^2 = {} & \chi^2_{\rm rate}(\sin^2 2\theta, \Delta m^2, N_{\rm BG1\sim 2}, \alpha_{1\sim 4}) \\ & -2\log L_{\rm shape}(\sin^2 2\theta, \Delta m^2, N_{\rm BG1\sim 2}, \alpha_{1\sim 4}) \\ & +\chi^2_{\rm BG}(N_{\rm BG1\sim 2}) + \chi^2_{\rm distortion}(\alpha_{1\sim 4}),\end{aligned}$$

where $L_{\rm shape}$ is the likelihood function of the spectrum including deformations from various parameters. $N_{\rm BG1\sim 2}$ are the estimated number of ^{9}Li and ^{8}He backgrounds and $\alpha_{1\sim 4}$ are the parameters for the shape deformation coming from energy scale, resolution, $\bar{\nu}_e$ spectrum and fiducial volume. These parameters are varied to minimize the χ^2 at each pair of $[\Delta m^2, \sin^2\theta]$ with a bound from $\chi^2_{\rm BG}(N_{\rm BG1\sim 2})$ and $\chi^2_{\rm distortion}(\alpha_{1\sim 4})$. The best fit to the KamLAND data in the physical region yields $\sin^2 2\theta = 1.0$ and $\Delta m^2 = 6.9 \times 10^{-5}$ eV^2 while the global minimum occurs slightly outside the physical region at $\sin^2 2\theta = 1.01$ with the same Δm^2.

These numbers can be compared to the best fit LMA values of $\sin^2 2\theta = 0.833$ and $\Delta m^2 = 5.5 \times 10^{-5}$ eV^2 from [30].

Another spectral shape analysis is performed with a lower prompt energy threshold of 0.9 MeV in order to check the stability of the above result and study the sensitivity to $\bar{\nu}_{\rm geo}$. With this threshold, the total background is estimated to be 2.91 ± 1.12 events, most of which come from accidental and spallation events. The systematic error is 6.0%, which is smaller than that for the final event sample due to the absence of an energy threshold effect. When the maximum likelihood is calculated, the $\bar{\nu}_{\rm geo}$ fluxes from ^{238}U and ^{232}Th are treated as free parameters. The best fit in this analysis yields $\sin^2 2\theta = 0.91$ and $\Delta m^2 = 6.9 \times 10^{-5}$ eV^2. These results and the allowed region of the oscillation parameters are in good agreement with the results obtained above. The numbers of $\bar{\nu}_{\rm geo}$ events for the best fit are 4 for ^{238}U and 5 for ^{232}Th, which corresponds to ~40 TW radiogenic heat generation according to model Ia in [25]. However, for the same model, $\bar{\nu}_{\rm geo}$ production powers from 0 to 110 TW are still allowed at 95% CL with the same oscillation parameters.

If three neutrino generations are considered, the $\bar{\nu}_e$ survival probability depends on two mixing angles θ_{12} and θ_{13}. In the region close to the best fit KamLAND solution the survival probability is, to a very good approximation, given by

$$P(\bar{\nu}_e \to \bar{\nu}_e) \cong \cos^4\theta_{13}\left[1 - \sin^2 2\theta_{12}\sin^2\frac{\Delta m^2_{12}L}{4E_\nu}\right], \qquad (2)$$

with $\Delta m_{12} \cong \Delta m^2$ from the 2-flavor analysis above. The CHOOZ experiment [31] established an upper limit of $\sin^2 2\theta_{13} < 0.15$, or $\cos^4\theta_{13} \geq 0.92$. The best fit KamLAND result would correspond approximately to $0.86 < \sin^2 2\theta_{12} < 1.0$.

In summary KamLAND has used measurements at large distances (~180 km) to demonstrate, for the first time, reactor $\bar{\nu}_e$ disappearance at a high confidence level (99.95%). Since one expects a negligible reduction of $\bar{\nu}_e$ flux from the SMA, LOW and VAC solar neutrino solutions, the LMA region is the only remaining oscillation solution consistent with the KamLAND result and CPT invariance. The allowed LMA region is further reduced by these results. Future measurements with greater statistical precision and reduced systematic errors will enable KamLAND to provide a high-precision measurement of the neutrino oscillation parameters.

6. KamLAND and solar neutrino data

Details [1] of combined fits of solar and KamLAND data will be discussed in Goswami's talk. Of course, one has to assume CPT in order to do this; in any case there is no evidence against CPT invariance. What is clear is that only the LMA solution is now viable. There are two mass (difference) values which are preferred: one at about 1.4×10^{-4} eV^2 and one at 7×10^{-5} eV^2 and the mixing in both cases at about $\tan^2\theta \sim 0.4$. All the unconventional scenarios are now ruled out and can only be sub-leading effects and can be constrained [18]. To check the LMA solution independently in solar neutrinos, the search for day–night effect in SNO CC data becomes important. With more data and reduction in systematic errors, KamLAND should be able to pin down δm^2 and also provide a measurement of geo-neutrinos.

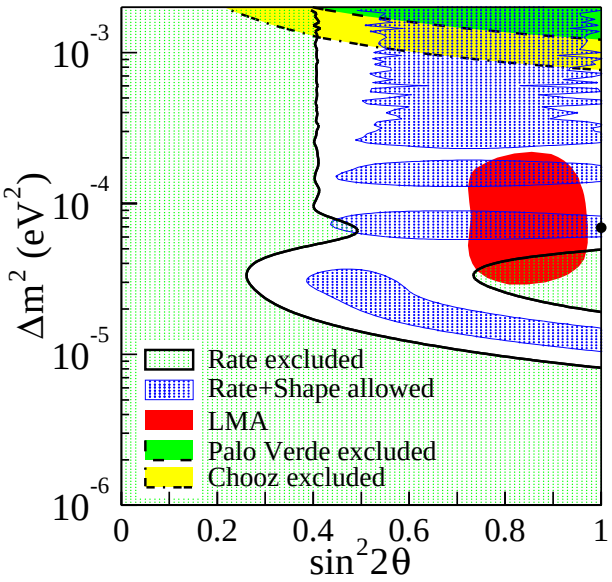

Figure 1. Excluded regions of neutrino oscillation parameters for the rate analysis and allowed regions for the combined rate and shape analysis from KamLAND at 95% CL. At the top are the 95% CL excluded region from CHOOZ [31] and Palo Verde [32] experiments, respectively. The 95% CL allowed region of the 'large mixing angle' (LMA) solution of solar neutrino experiments [30] is also shown. The thick dot indicates the best fit to the KamLAND data in the physical region: $\sin^2 2\theta = 1.0$ and $\Delta m^2 = 6.9 \times 10^{-5}$ eV^2. All regions look identical under $\theta \leftrightarrow (\pi/2 - \theta)$ except for the LMA region.

7. LSND

There exists a combined analysis of the final LSND and KARMEN results [33]. This allows a thin slice of parameter range for explanation of LSND results in terms of oscillations: $\delta m^2 \sim$ (0.2–1) eV^2 and $\sin^2 2\theta \sim$0.03–0.003; there is also an allowed point at $\delta m^2 \sim 7$ eV^2 and $\sin^2 2\theta \sim 0.004$.

The conventional way to accommodate LSND result is to invoke a fourth sterile neutrino. The four masses can be arranged in two basic patterns: $3+1$ or $2+2$. In the $3+1$ case, the conversion probability is given by

$$P_{\mu e} = A_{\mu e} \sin^2(\delta m^2 L/4E), \tag{3}$$

where $A_{\mu e} = 4U_{\mu 4}^2 U_{e4}^2$ and is constrained severely by CDHS, BUGEY and CHOOZ data. These constraints strongly disfavor if not rule out this possibility [34]. The other pattern 2+2 is constrained by the fact that the total probability in both solar and atmospheric data for the presence of sterile neutrino is less than about 75% [35]. Naively, this should be 100% but allowing a general 4×4 mixing matrix loosens the constraints. The current situation is that this scenario while disfavored, is not ruled out [36]. The oscillation interpretation of LSND will be tested by the on-going Mini-Boone experiment at Fermilab; with two years of running [37].

In order to avoid the sterile neutrino, it was proposed to violate CPT invariance in neutrino mass matrix and have the LSND mass difference in $\bar{\nu}$ sector and solar mass difference in the ν sector [38]. But the KamLAND observation of LMA rules out this proposal. A revised proposal is that the KamLAND and solar δm^2 may not be identical and have the KamLAND and LSND mass splittings in the $\bar{\nu}$ sector but no atmospheric δm^2 in the $\bar{\nu}'s$ [39]. This is not yet ruled out and can be tested in the future, e.g. Mini-Boone should see the LSND effect only in the $\bar{\nu}$ channel; the solar and KamLAND δm^2-mixing should not be identical, eventually see the effects in the atmospheric neutrino data as well as future long baseline experiments. There are some theoretical questions posed by this proposal, such as how much Lorentz invariance violation is implicit from virtual CPT violation in the loops, which remain open. A different proposal for explaining the LSND is that it is due to a rare decay mode of μ, violating lepton number by two units.

$$\mu^+ \to e^+ \bar{\nu}_e \bar{\nu}_\alpha \quad (\alpha = e, \mu \text{ or } \tau) \tag{4}$$

with a branching ratio of about 2×10^{-3}. Extensions of standard model can be constructed which can give rise to this mode at such a level and are consistent with all other data [40]. Tests for this proposal are: (i) Mini-Boone should see no evidence for $\nu_\mu \to \nu_e$ (or $\bar{\nu}_\mu \to \bar{\nu}_e$) since the source for $\nu'_\mu s$ is π decays and not μ decays; (ii) there are scalar mesons in the range of 300–500 GeV with specific properties (e.g. $H^{++} \to \ell^+\ell^+$) which should be detectable at LHC; (iii) since the effective interaction of $\Delta L = 2$ mode has a different space-time structure than $(V-A)^2$, the Michel parameters are modified. For example ρ changes from $\rho = 3/4$ to $\rho_{\text{eff}} = 3/4(1-\epsilon)$, where ϵ is the branching ratio. The ongoing experiment TWIST (at TRIUMF) will measure ρ to a level of 10^{-4} and even with radiative corrections (at a level 10^{-4}), should be able to test this deviation from 3/4 [41]. Already the new limit from KARMEN for such a mode is 1.7×10^{-3} whereas LSND requires a rate no lower than 1.8×10^{-3} at two s.d. and so this explanation is getting tightly squeezed [42]. The bottom line is that all explanations of LSND live dangerously!

8. Conclusion

I did not have time to discuss the questions about absolute masses of neutrinos from tritium end-point measurements or double beta decay results or the determination of total mass in neutrinos from cosmological measurements. The form of the MNS mixing matrix for the three flavor is now fairly well-determined with some obvious gaps. The mass matrix poses a big challenge to theory. Is the smallness of the masses a real problem? Is see-saw the right way to go? Is the mass of Majorana nature? Quasi-degeneracy or quasi-hierarchy? Inverted or normal? These are theoretical as well as experimental questions. Many theoretical proposals exist, none is as yet compelling; we will hear about these in Mahopatra's talk [43]. What we would like to learn over the next few years is quite clear. Here is a wish-list:

(i) To see the oscillation dips in atmospheric neutrinos and in KamLAND $\bar{\nu}'_e s$; (ii) to measure the solar $\nu'_e s$ over the whole energy spectrum. (iii) to determine U_{e3}; (iv) to determine if CPV effects are large and measure δ if possible; (v) to detect $\nu'_\tau s$ in $\nu_\mu \to \nu_\tau$ oscillations; (vi) to settle the LSND question; (vii) to measure the

absolute neutrino masses (determine if the mass hierarchy is normal or inverted); (viii) to determine Majorana versus Dirac nature; (ix) to see high energy $\nu's$ from astrophysical sources, (x) to determine if neutrinos decay; (xi) to observe cosmological background neutrinos; and so forth. Goodman will discuss future experiments which will attempt to cover some of these things [44].

Acknowledgements

I offer all the collaborators on KamLAND my congratulations for the outstanding performance of the detector (as well as the exciting results). This work was supported in the past by the US DOE under DOE Grant DE-FG 03 94ER40833.

References

[1] S Goswami, *Pramana – J. Phys.* **62**, 241 (2004)
[2] NuTeV Collaboration: G P Zeller *et al*, *Phys. Rev. Lett.* **88**, 091802 (2002)
[3] C V Achar *et al*, *Phys. Lett.* **B18**, 196 (1965)
[4] F Reines *et al*, *Phys. Rev. Lett.* **15**, 551 (1965)
[5] M R Krishnaswamy *et al*, *Proc. R. Soc. London* **A323**, 489 (1971)
F Reines *et al*, *Phys. Rev.* **D4**, 80 (1971)
L V Volkova and G T Zatsepin, *Yad. Fiz.* **14**, 117 (1972)
[6] V Barger, K Whisnant, D Cline and R J N Philips, *Phys. Lett.* **B93**, 194 (1980)
[7] T J Haines *et al*, *Phys. Rev. Lett.* **57**, 1986 (1986)
[8] K S Hirata *et al*, *Phys. Lett.* **B205**, 416 (1988)
[9] V Barger and K Whisnant, *Phys. Lett.* **B209**, 365 (1988)
J G Learned, S Pakvasa and T Weiler, *Phys. Lett.* **B209**, 79 (1988)
K Hidaka, M Honda and S Midorikawa, *Phys. Rev. Lett.* **61**, 1537 (1988)
[10] R Becker-Szendy *et al*, *Phys. Rev. Lett.* **69**, 1010 (1992)
[11] K S Hirata *et al*, *Phys. Lett.* **280**, 146 (1992)
[12] S L Glashow, in *Quarks and leptons*, Cargese 1979, edited by M Levy *et al* (Plenum, New York, 1980) p. 707
[13] S Pakvasa, in *Proc. of 1980 International DUMAND Symposium*, Honolulu, HI, 1981, vol. II, p. 45
[14] Y Fukuda *et al*, *Phys. Rev. Lett.* **81**, 1562 (1998)
[15] M Shiozawa, *Proceedings of the XXth International Conference on Neutrino Physics and Astrophysics*, Munich, June, 2002
[16] M Goodman, hep-ex/0210055
[17] B J Kim *et al*, *Phys. Rev. Lett.* **90**, 041801 (2003)
[18] S Pakvasa and J Valle, hep-ph/0301061 and references therein
[19] K Eguchi *et al*, *Phys. Rev. Lett.* **90**, 021802 (2003)
[20] A Suzuki, talk at the *XVIII International Conference on Neutrino Physics and Astrophysics*, Takayama, Japan, 1998 and its proceedings
http://www.awa.tohoku.ac.jp/KamLAND/
[21] F Reines and C L Cowan, *Phys. Rev.* **92**, 830 (1953)
[22] K S Hirata *et al*, *Phys. Rev.* **D38**, 448 (1988)
[23] J B Benziger *et al*, *Nucl. Instrum. Methods* **A417**, 278 (1998)
[24] H Kume *et al*, *Nucl. Instrum. Methods* **205**, 443 (1986)

[25] R S Raghavan *et al*, *Phys. Rev. Lett.* **80**, 635 (1998)
[26] T Hagner *et al*, *Astropart. Phys.* **14**, 33 (2000)
[27] ^{235}U: K Schreckenbach *et al*, *Phys. Lett.* **B160**, 325 (1985)
^{239,241}Pu: A A Hahn *et al*, *Phys. Lett.* **B218**, 365 (1989)
^{238}U: P Vogel *et al*, *Phys. Rev.* **C24**, 1543 (1981)
[28] B Achkar *et al*, *Phys. Lett.* **B374**, 243 (1996)
G Zacek *et al*, *Phys. Rev.* **D34**, 2621 (1986)
[29] http://www.insc.anl.gov/
[30] G L Fogli *et al*, *Phys. Rev.* **D66**, 053010 (2002)
[31] M Apollonio *et al*, *Phys. Lett.* **B466**, 415 (1999)
[32] F Boehm *et al*, *Phys. Rev.* **D64**, 112001 (2001)
[33] E D Church *et al*, *Phys. Rev.* **D66**, 013001 (2002)
[34] M Maltoni *et al*, *Nucl. Phys.* **B643**, 321 (2002)
[35] O L G Peres and A Smirnov, *Nucl. Phys.* **B599**, 3 (2001)
E Akhmedow, *Proc. of XXth International Conf. on Neutrino Physics and Astrophysics*, Munich, June 2002
[36] H Pas, L-G Gons and T Weiler, *Phys. Rev.* **D67**, 073019 (2002)
[37] http://www-boone.fnal.gov
[38] H Murayama and T Yanagida, *Phys. Lett.* **B520**, 263 (2001)
G Barenboim *et al*, *J. High Energy Phys.* **0210**, 001 (2002)
[39] G Barenboim, L Borisov and J Lykken, hep-ph/0212116
[40] K S Babu and S Pakvasa, hep-ph/024236
[41] http://twist.phy.ualberta.ca/roddning/E614/
[42] B Armbruster *et al*, hep-ex/0302017
[43] R N Mohapatra, *Pramana – J. Phys.* **62**, 319 (2004)
[44] M Goodman, *Pramana – J. Phys.* **62**, 229 (2004)